

Article

Not peer-reviewed version

# Integrated use of SAR and Optical data in mapping native vegetation: a study in a transitional Brazilian Cerrado-Atlantic Forest interface

[Allita Rezende Santos](#)\*, [Mariana Abibi Guimarães Araujo Barbosa](#), [Phelipe da Silva Anjinho](#),  
Denise Parizotto, Frederico Fabio Mauad

Posted Date: 4 June 2024

doi: 10.20944/preprints202406.0170.v1

Keywords: backscattering coefficients; multi-sensor optimizing; Synthetic Aperture Radar



Preprints.org is a free multidiscipline platform providing preprint service that is dedicated to making early versions of research outputs permanently available and citable. Preprints posted at Preprints.org appear in Web of Science, Crossref, Google Scholar, Scilit, Europe PMC.

Copyright: This is an open access article distributed under the Creative Commons Attribution License which permits unrestricted use, distribution, and reproduction in any medium, provided the original work is properly cited.

*Article*

# Integrated Use of SAR and Optical Data in Mapping Native Vegetation: A Study in a Transitional Brazilian Cerrado-Atlantic Forest Interface

Allita Santos <sup>1,\*</sup>, Mariana Barbosa <sup>2</sup>, Phelipe Anjinho <sup>3</sup>, Denise Parizotto <sup>4</sup> and Frederico Mauad <sup>5</sup>

<sup>1</sup> Center for Water Resources and Environmental Studies (CRHEA), University of São Paulo, São Carlos 13566-590, SP, Brazil

<sup>2</sup> mariana.abibi@usp.br

<sup>3</sup> phelipe.anjinho@usp.br

<sup>4</sup> deniseparizotto@usp.br

<sup>5</sup> mauad.ffmpeg@sc.usp.br

\* Correspondence: allita@usp.br; Tel.: +55-(41)-99233-0185

**Abstract:** This study develops a structure for mapping native vegetation in a transition area between Brazilian Cerrado and Atlantic Forest from integrated spatial information from the Sentinel-1 and Sentinel-2 satellites. Most studies use this data separately, however, the integrated use of optical sensors with Synthetic Aperture Radar (SAR) sensors can improve the methodology for classifying land use and land cover (LULC). The fusion of Sentinel-1 and Sentinel-2, for example, can increase the accuracy of mapping algorithms, using complementary information, such as spectral, backscattering, polarimetry, and interferometry. The study area comprises the Lobo Reservoir Hydrographic Basin, which is part of an environmental conservation unit protected by Brazilian law and with significant human development. LULC were classified, using the random forest deep learning algorithm. The classifying attributes were backscatter coefficients, polarimetric decomposition, and interferometric coherence for radar data (Sentinel-1), and optical spectral data, comprising bands in the red edge, near infrared, and shortwave infrared (Sentinel-2). The attributes were evaluated in three settings in which the SAR and optical data were evaluated separately (C1 and C2, respectively) and in an integrated manner (C3). The study found greater accuracy for C3 (96.54%), an improvement of nearly 2% compared to C2 (94.78%) and more than 40% in relation to C1 (55.73%). The classification algorithm encountered significant challenges in identifying wetlands in C1, but performance improved in C3, enhancing differentiation by stratifying a greater number of classes during training and facilitating visual interpretation during sampling. Accordingly, the use of SAR and optical data becomes an alternative to optimize LULC mapping in tropical regions, due to the limited influence of atmosphere on images in the microwave range.

**Keywords:** backscattering coefficients; multi-sensor optimizing; synthetic aperture radar

## 1. Introduction

Alterations in land use and land cover (LULC) arising from anthropic activities are one of the principal environmental problems studied by scientists [1–6]. Adverse changes in conservation areas cause environmental damage and harm our quality of life, such as reduction in the available water for human consumption, or reduction in soil nutrients for food production. [4]. Society is highly dependent on a functional and stable land system for food production and access to natural resources, including water, timber, fiber, ore, and fuel, among other ecosystem services [5,7]. In this instance, the functionality and stability of land systems depend on the interaction of soil, water, and plants within the ecological composition and the quality of native vegetation [8,9]. Thus, mapping the composition of vegetation, not only provides information on the region's quantitative and qualitative

state, but is a crucial initial step in the analyzing and monitoring its management, including the state of the natural vegetation and the impact of anthropic activities on affected ecosystems [10].

The Brazilian Cerrado biome is a global biodiversity hotspot. It encompasses three of South America's largest river basins (Amazon, São Francisco, and Prata), contributing nearly half Brazil's surface water and recharging the Bambuí, Urucuia, and Guarani aquifers, which depend on its integrity [11]. Its vital significance for the conservation of species and the provision of ecosystem services notwithstanding, only 53.1% of its original area has been preserved [12], as it lost 279,000 km<sup>2</sup> between 1985 and 2021 from LULC changes arising from such anthropic endeavors as crops, pastures, forestry, mining, industrialization, and human expansion [12].

A similar trend can be observed in the Atlantic Forest, where 70% of Brazilians live, as only 24.3% remains as a forest formation [13]. The forest largely corresponds to the legal reserve and permanent protection areas (PPAs), whose role is to preserve the quality of water, soil and, biodiversity [4,8,9]. The quality of the vegetation cover has also been adversely impacted, as there was a 23% loss of mature forest from 1985 to 2021 [5]. In 37 years, 98,000 km<sup>2</sup> of primary vegetation were suppressed, while 88,000 km<sup>2</sup> regenerated into secondary vegetation [13], which comprises 26% of forest cover in the Atlantic Forest. Thus, mapping the spatial composition of forest vegetation is fundamental for the evaluation of the spatial pattern of ecosystem services in an environmental study[10].

Without adequate LULC management focused on sustainability, regional river basins suffer persistent alterations. The Lobo Reservoir Hydrographic Basin (LRHB), hereafter basin, is formed by streams and rivers that contribute to the reservoir [2–4,14]. It lies in the center-west of the state of São Paulo, Brazil, a transitional region between the Brazilian Cerrado and the Atlantic Forest, over 200 km from the city of São Paulo, one of the principal financial, corporate, and commercial centers of South America [4,14]. The state encompasses just 16.6% and 28.4% of the two biomes, respectively [12,13].

Algorithms using machine learning can efficiently classify images from remote sensing and are capable of handling high-dimensional data and map thematic classes with complex features [15]. As remote sensing can provide cost-efficient data, it is suitable for LULC evaluation at higher spatial resolution. The free availability of medium-high spatial resolution imagery, such as Sentinel-1 radar data and Sentinel-2 optical data, can facilitate mapping the state of native vegetation in regions where ecosystem services require finer-scale assessments [16]. Several studies have examined the applicability of active synthetic aperture radar (SAR) to map LULC in terms of specific objectives [10,16–23]. One study delineated cocoa agroforests in Cameroon from textural features extracted from SAR imaging [22], and another evaluated the value of short-time baseline coherence of SAR images over a complex agricultural area in the state of São Paulo [21]. With all-day and all-weather operational capability, these sensors provide diverse, complementary physical data that enhances spectral data when combined with optical imaging [10,16,19,23]. In addition, the fusion of Sentinel-1 and Sentinel-2 increased the accuracy of LULC mapping, using complementary information, such as spectral [18,20], backscattering, polarimetry, and interferometry [17].

However, the works in general has been carried out to map vegetated and non-vegetated areas without distinction in relation to the type of vegetation characteristic of the region under study. Furthermore, the mappings carried out in studies and published in high-impact journals have not yet explored the expanded extraction of LULC thematic classes with the intention of differentiating types of transitional vegetation between different biomes, and reforestation for commercial and research purposes. In Brazil, research has focused on mapping the vegetation characteristic of the Amazon Forest, thus leaving other biomes with tropical characteristics without scientific reference. Therefore, this study seeks to fill the gaps in the field of remote sensing using multi-sensor and spatial data typology.

Regarding remote sensing LULC mapping, advanced artificial neural networks, especially deep learning models, have gained increased attention due to their end-to-end nature [16]. An obstacle affecting the performance of deep learning networks is the dearth of training samples [24]. Accordingly, a framework based on deep learning for classifying native vegetation in the transitional

regions that can integrate SAR and optical data and effectively handle training samples should be developed.

This study develops such an architecture for mapping native vegetation from integrated spatial information from the Sentinel-1 and Sentinel-2 satellites. To this end, the Lobo Reservoir Hydrographic Basin, which is located in an environmental conservation unit protected by Brazilian law for the purpose of sustainable use, was adopted as its study area, as it is a region with significant agricultural, mining, and industrial development. The spatial composition of the basin's native vegetation is formed by permanent protection areas, consisting of fragments of the Atlantic Forest in regions of rivers and streams, close to springs and the region comprising the Ecological Station of Itirapina composed of vegetation characteristic of the typical savannah and grassland Brazilian Cerrado biome. The study further contributes to national and international research, as the basin is part of the long-term ecological research program of the National Council for Scientific and Technological Development, which promotes advances in environmental and ecological research [2–4,8,14,25,26].

## 2. Materials and Methods

The study's methodology is characterized as follows. Section 2.1 presents the characterization of the study area and section 2.2 describes the source and acquisition of spatial data used to elaborate the LULC map. Section 2.3 describes the elaboration of LULC classification attributes derived from the integration of optical and SAR data, while Section 2.4 delineates the classification of the LULC map and the evaluation of the accuracy of the architecture developed from the field visit.

### 2.1. Study Area

Located in the center-west region of the state of São Paulo, between Brotas and Itirapina, at the geographic coordinates 22°15'S and 47°49'W (Figure 1), the Lobo Reservoir Hydrographic Basin (LRHB), officially designated the Carlos Botelho Reservoir, has an area of 230 km<sup>2</sup>, drainage density of 0.75 km/km<sup>2</sup>, maximum altitude of 800 meters and slope of 0.0075 m/m [8].

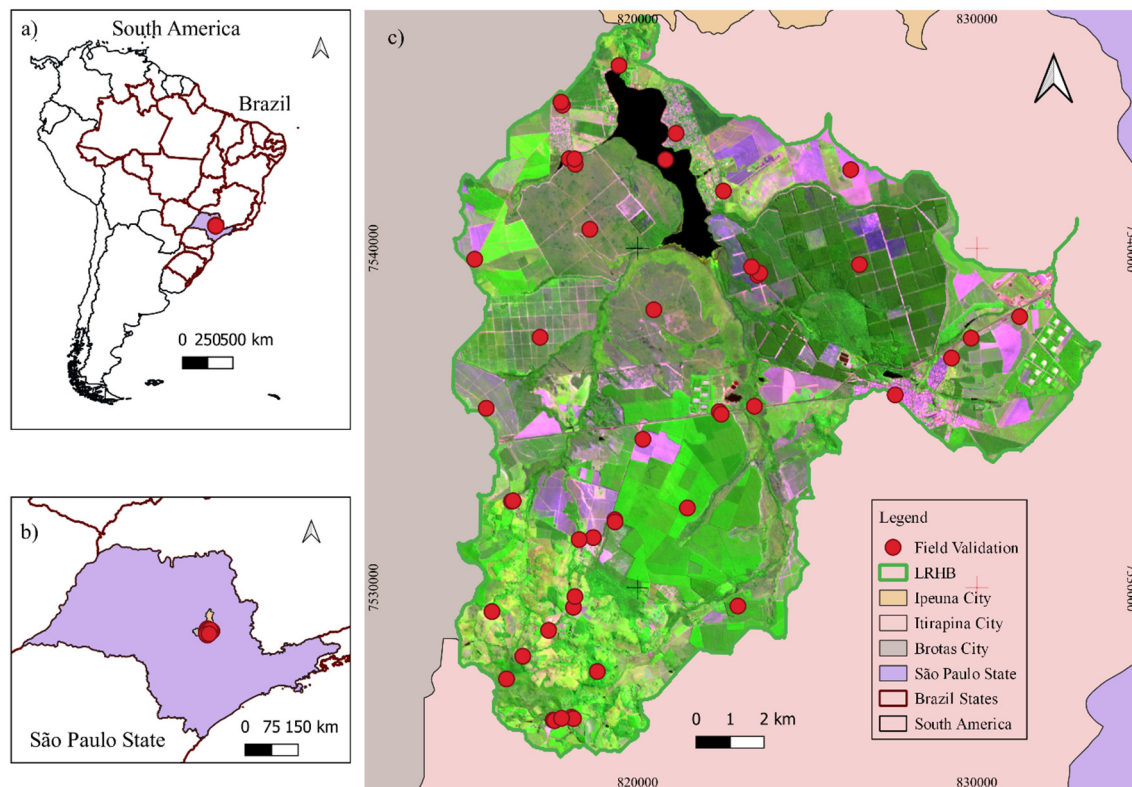


**Figure 1.** Lobo Reservoir Hydrographic Basin localization and points used to field validation.



Constructed in 1936 to generate electricity, the Lobo Reservoir is currently used for irrigation, tourism, and research. One of Brazil's most studied reservoirs, it is known worldwide as the Broa model, reflecting the scientific research it has generated since the 1970s as a strategic project of two major universities, the University of São Paulo, and the Federal University of São Carlos [2–4,14,25]. The reservoir is primarily formed by contributions of the Itaqueri river and the Lobo stream, augmented by contributions from the Água Branca, Geraldo, Limoeiro, and Perdizes streams. The region is in the Tietê/Jacaré Water Resources Management Unit (number 13) and part of the Tietê river basin and, consequently, those of the Paraná and Prata rivers.

The basin is in the special use region of the Corumbataí Environmental Protection Area, created by State Decree 20,960 [27]. Among its ecological attributes, its highly diverse natural environments, rich historical and archaeological heritage, quality hydrological resources, and scenic landscape stand out. The protection area seeks to regulate development ensuring the basin's sustainability through sustainable use, which balances the use of natural resources with their conservation.

The Itirapina Ecological and Experimental Stations are also located in the basin and are under the Brazilian Forestry Institute. The former station was created by State Decree 22,335 in 1984 and the later by expropriation decrees. The stations focus on environmental preservation and conservation through forestry management, environmental education, research, visitation, and control of such activities such as agriculture, hunting, fishing, road construction, fire, and vandalism. The ecological station has a crucial role in conserving the Brazilian Cerrado, a typically savannah and grassland biome. Marked by characteristics of soil and climate, it includes formations originated during the glacial periods in which the global temperature dropped, and the climate became drier, favoring the retraction of forests and, consequently, the expansion of a more open vegetation, which required less moisture [28].

### 2.1. Spatial data used to evaluate LULC and classify native vegetation.

Table 1 details spatial data used for LULC evaluation and classification of native vegetation in transitional regions between the Brazilian Cerrado and Atlantic Forest interface.

**Table 1.** Types of data, source, acquisition date, and resolution used to compile the LULC map.

Data	Source	Acquired	Acquisition	Resolution
LULC	Sentinel 1 image	12/19/2022	[29]	5 x 20 m
		12/31/2022		
	Sentinel 2 image	3/25/2023	[29]	20 m
Waterways	Digital Elevation Model, Advanced Spaceborne Thermal Emission and Reflection Radiometer	2015	[30]	1:50.000
LRHB contour				

The LULC map was compiled from two single-look complex (SLC) images from Sentinel-1A (C band) in interferometric wide-swath (IW) mode, in descending orbit and in VV-VH polarizations to obtain the following attributes from radar data: backscatter coefficients ( $\sigma^{0}_{VH}$  e  $\sigma^{0}_{VV}$ ), polarimetric decomposition entropy (H) and alpha ( $\alpha$ ) and, interferometric coherence ( $\gamma_{VH}$  e  $\gamma_{VV}$ ) [17,31,32]; and an image with the 20 m spectral bands: red edge (B05, B06, B07, and B8A), near infrared (B08) and shortwave infrared (B11 and B12) of the Sentinel-2A satellite sensors to derive attributes from optical data. The images, dated September 19 and 31, 2022 for the radar images and March 25, 2023, for the optical image, were obtained free of charge from the website of the Copernicus Open Access Hub of the European Space Agency [29]. The study used radar data to the maximum extent and supplemented it with optical data to enhance LULC classification.

### 2.2. LULC classification attributes from integrated optical and SAR data

Sentinel-1A data was pre-processed using SNAP 8.0 software to obtain SAR attributes and R software to obtain optical attributes. As the study's assessment of the spatial composition of native

vegetation in transitional regions between the Brazilian Cerrado and Atlantic Forest interface was confined to the LRHB, the spatial pattern of its water ecosystem services could be examined with greater accuracy. The digital elevation model (DEM) obtained free of charge from the European Space Agency's Copernicus Open Access Hub website [29], collected by the Advanced Spaceborne Thermal Emission and Reflection Radiometer (ASTER) sensor in the year 2015 [30]. The outline of the hydrographic basin was attained from DEM to demarcate the study area and drainage network of waterways. Figure 2 depicts the pre-processing of LULC classification.

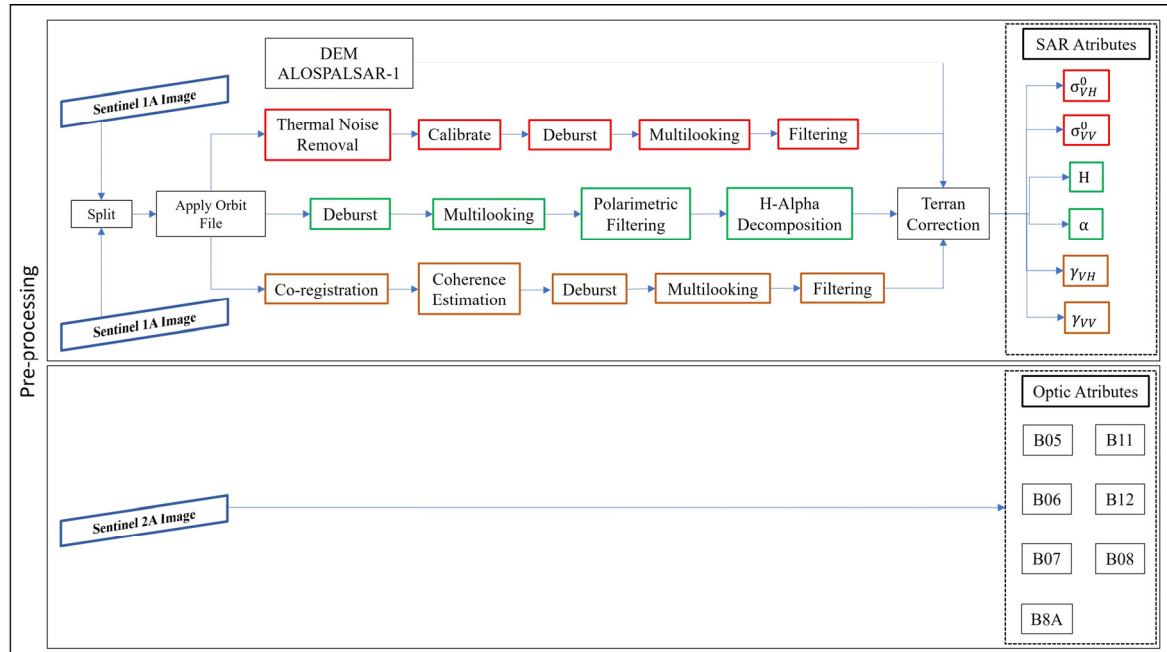


**Figure 2.** Pre-processing flowchart of LULC classification.

In the initial pre-processing step, the two Sentinel-1A SLC images were sub-configured through split processing considering the bandwidth covering the LRHB extension and to minimize SNAP data processing time. Apply Orbit File was applied to this subset to update the information in the image metadata. To determine the backscatter values ( $\sigma^{0}_{VH}$  e  $\sigma^{0}_{VV}$ ) thermal noise removal was applied to the sub-bands, followed by radiometric calibration. This process consists of transforming the digital numbers of the image into backscatter values per area ( $\sigma^0$ , Equation (1)), where  $DN_i$  are the pixels' digital numbers,  $A_i$  is an absolute calibration constant found in Look Up Table (LUTs) products and  $i$  represents the pixels.

$$\sigma_{eu}^0 = \frac{DN_{eu}^2}{A_{eu}^2} \quad (1)$$

The  $2 \times 2$  ( $T_{dual}$ ) coherence matrix was created using dual polarization data to attain the entropy (H) and alpha ( $\alpha$ ) polarimetric decomposition attributes. Cloude [33], proposed it as an adaptation of the  $3 \times 3$  coherence matrix applied to quad-pol data and implemented in SNAP (Equations (2) and (3)):

$$T_{dual} = \begin{pmatrix} T_{11} & T_{12} \\ T_{21} & T_{22} \end{pmatrix} = U \begin{bmatrix} \lambda_1 & 0 \\ 0 & \lambda_2 \end{bmatrix} U^H = \lambda_1 u_1 u_1^H + \lambda_2 u_2 u_2^H \quad (2)$$

$$H = -\sum_{i=1}^2 (P_i \log_2 P_i) \quad \text{and} \quad \alpha = \sum_{i=1}^2 P_i \cos^{-1} (|u_{1i}|) \quad (3)$$

where  $P_i$  represents the relative importance of the eigenvalues of the coherence matrix ( $\lambda_i$ ) and is obtained from Equation (4):

$$P_i = \frac{\lambda_i}{\sum_{j=1}^2 \lambda_j} \quad i = 1, 2 \quad (4)$$

The two Sentinel-1A images were acquired within 12 days, allowing co-registration to obtain interferometric coherence ( $\gamma_{VH}$  e  $\gamma_{VV}$ ). The interferometric coherence calculation (Equation (5)) was performed using a  $10 \times 3$  window.

$$\gamma = \frac{|(S_1(x)S_2(x))|}{\sqrt{(|S_1(x)|^2)(|S_2(x)|^2)}}$$

(5)

where  $\gamma$  represents the interferometric coherence,  $S_1$  and  $S_2$  are the co-registered SLC images, and  $\langle \rangle$  is the mean over window size.

Deburst processing was applied to merge the subtracts, Multilook ( $4 \times 1$  looks) and Lee filter with  $3 \times 3$  window [34] for speckle noise reduction. Finally, the topographic correction of the SAR attributes was performed with Range Doppler Terrain Correction, using the DEM Alos-PalSAR-1, with 12.5 m spatial resolution, from Alaska Satellite Facilities.

2.3. Image classification and accuracy assessment

The LULC map was generated with the Random Forest (RF) machine learning algorithm [35,36] using R 2.07.2022 software and the SIRGAS 2000 geodetic reference system in the Universal Transversal Mercator cartographic projection, Zone 23 South. For RF, the parameters Ntree were defined as 500 and Mtry as the square root of the number of input variables. Ten training samples were collected for each land use class, identified according to expressive distribution. The identified classes were agriculture, water (reservoir), wetlands, urban area, Brazilian Cerrado, native vegetation (Atlantic Forest), pasture, experimental reforestation (Itirapina Experimental Station), productive reforestation (wood production), and exposed soil. The study classified native vegetation of the Brazilian Cerrado and experimental reforestation distinctly from productive reforestation to better understand the relevance of each type of activity that uses land for economic and social development.

To evaluate the use of attributes from the Sentinel-1A and Sentinel-2A satellites in LULC mapping, three sets were classified and compared, using the attributes separately for SAR and optical data and combined (Table 2).

Table 2. Evaluation of SAR and optical attributes separately and combined.

Set	Attributes	Data type
C1	$\sigma^{0}_{VH} + \sigma^{0}_{VV} + H + \alpha + \gamma_{VH} + \gamma_{VV}$	SAR
C2	B05 + B06 + B07 + B08 + B8A + B11 + B12	Optical
C3	$\sigma^{0}_{VH} + \sigma^{0}_{VV} + H + \alpha + \gamma_{VH} + \gamma_{VV}$ + B05 + B06 + B07 + B08 + B8A + B11 + B12	Combined

From field observations at forty-seven points (Figure 1) widely distributed in the basin, new pixel samples were collected for precision tests related to each LULC class as a field reference [37–39]. The field visit was conducted on April 23, 2023. The elaboration of the LULC map was used interpretation of high-resolution satellite images with optical and radar data, through the RGB combination of spectral bands and radar, in addition to high-resolution images via Google Earth [4,14,40]. The results were analyzed using a confusion matrix to evaluate the accuracy of a classification by comparing it with field reference data [37–39]. From the transition matrix of the reference and prediction data, the producer and user accuracy values, omission, and inclusion errors for each class, as well as the overall classification accuracy, were identified.

### 3. Results

#### 3.1. Detailed LULC Classification for Integrated SAR and Optical Data

Figure 3 uses boxplot graphs to depict class separability with SAR attributes and optical data from Sentinels 1A and 2A, with upper, lower, median, mean, maximum, and minimum values for each class. Regarding the former (SAR attributes), the urban area class evidenced the highest separability, while in the case of the latter (optical attributes), urban area, pasture, exposed soil, and water showed the greatest variation.

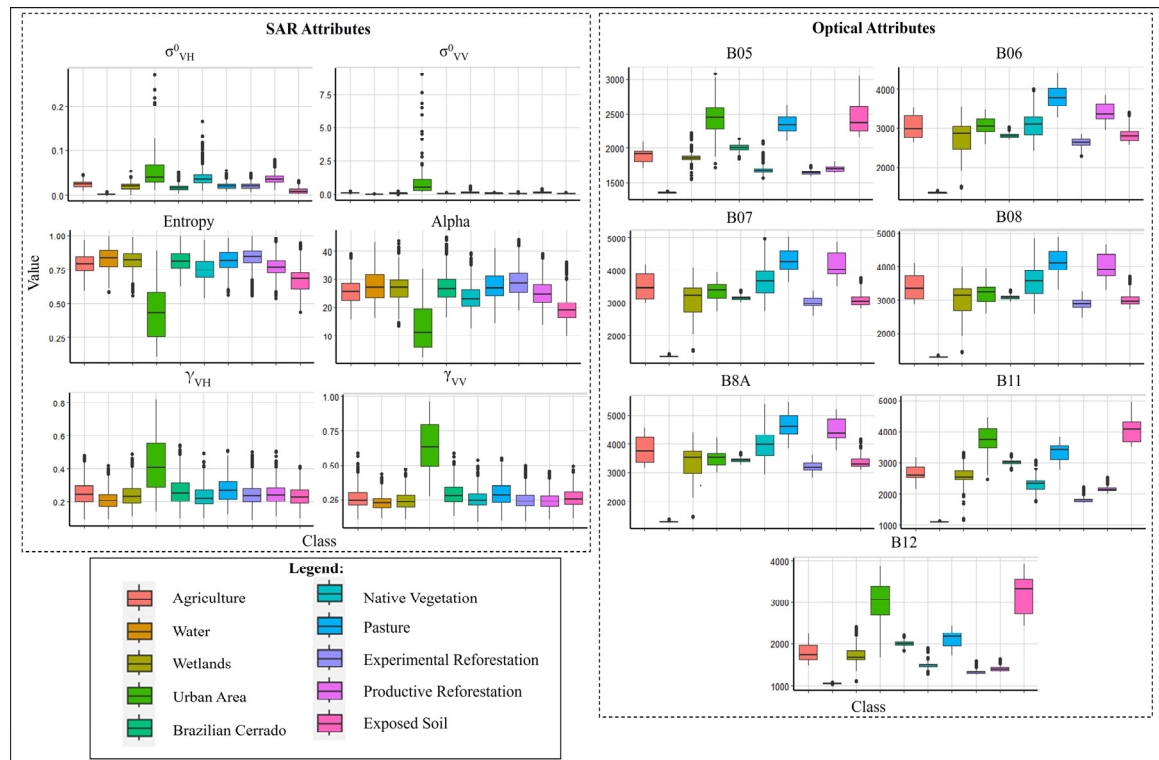


**Figure 3.** SAR attributes and optical data with values for each class.

Figure 4 depicts values for each band. This fundamental RF algorithm result shows the importance of each attribute in classifying data. The figure plots mean decrease accuracy (MDA) to show the precision the model loses by excluding each variable. Accordingly, the more a variable decreases precision, the greater its importance for sound classification. The mean decrease gini (MDG) is a measure of how each variable contributes to the homogeneity of nodes and leaves in RF. The greater the precision value of its MDA or MDG rating, the greater the importance of the variable in the model. In Figure 4, it is observed that when SAR data are used exclusively (C1), the importance values are high, highlighting the backscatter coefficients ( $\sigma^{0}_{VH}$  e  $\sigma^{0}_{VV}$ ). When it is integrated with optical data, greater homogeneity is observed for MDA importance values. MDG importance values, however, demonstrate that integrating SAR and optical data (C3) resulted in high use of optical data, with emphasis on spectral bands B05, B11 and B12, while still using SAR attributes, with emphasis on the backscatter coefficients ( $\sigma^{0}_{VH}$  e  $\sigma^{0}_{VV}$ ).



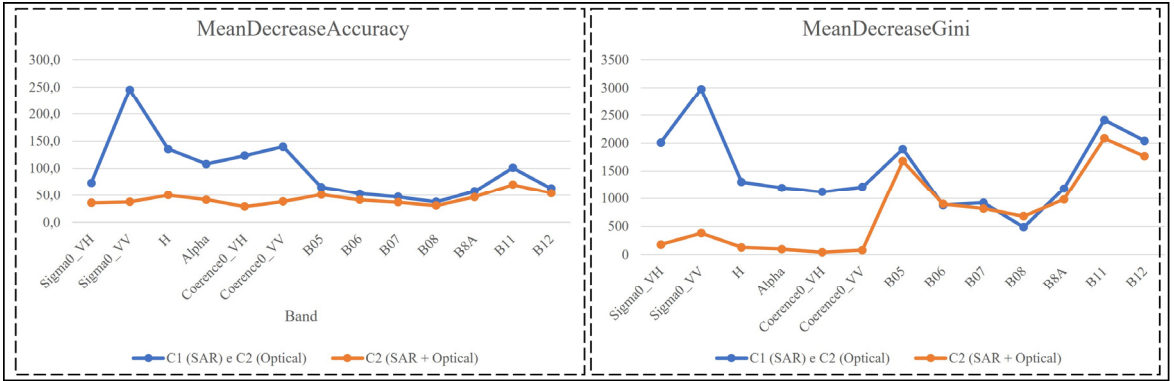


Figure 4. Importance of variables for mean decrease accuracy and mean decrease gini.

Figure 5 depicts RGB band compositions for C1, C2, and C3. The C1 bands present greater homogeneity in differentiating classes, enabling differentiation of water, pasture, urban area, and native vegetation, while the C2 bands present greater heterogeneity, which facilitates the collection of RF training samples. Finally, the C3 bands clearly differentiate the classes, highlighting distinctions between experimental and productive reforestation, native vegetation and Brazilian Cerrado, exposed soil and wetlands.

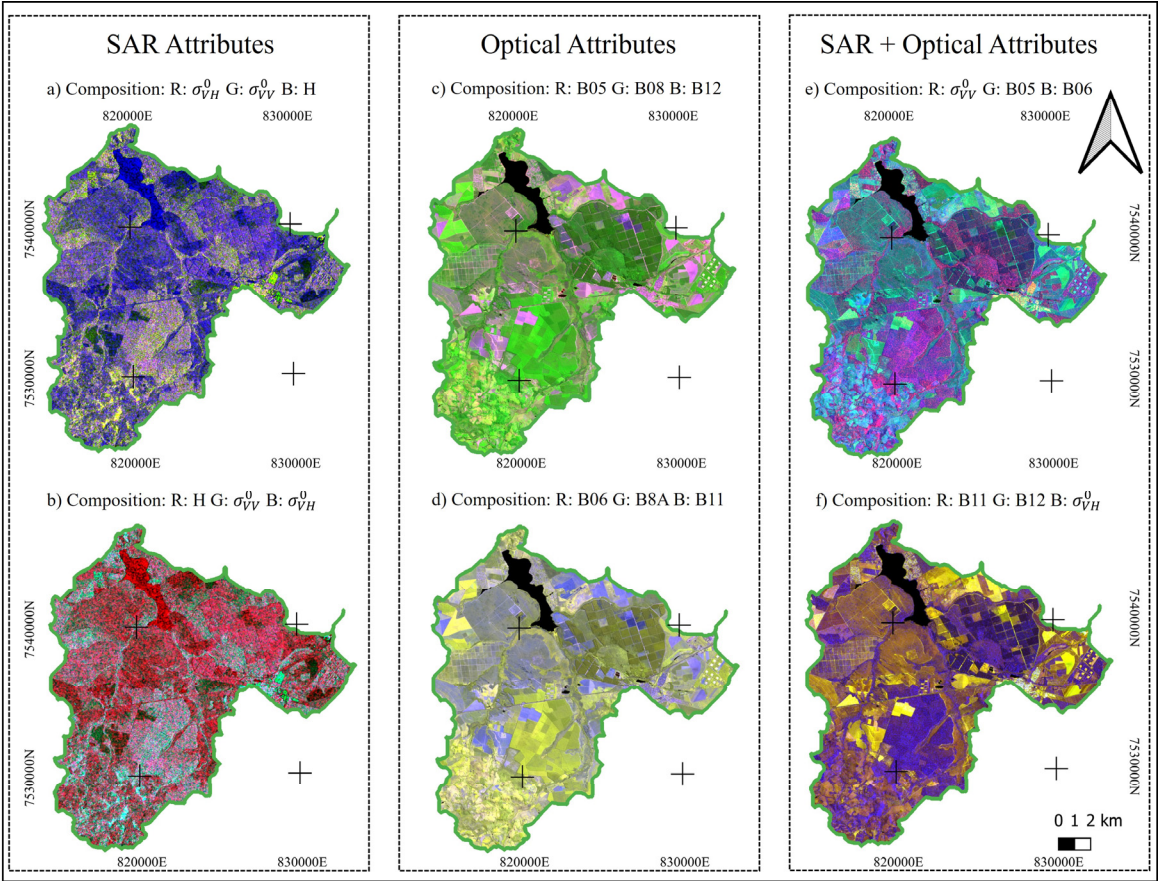
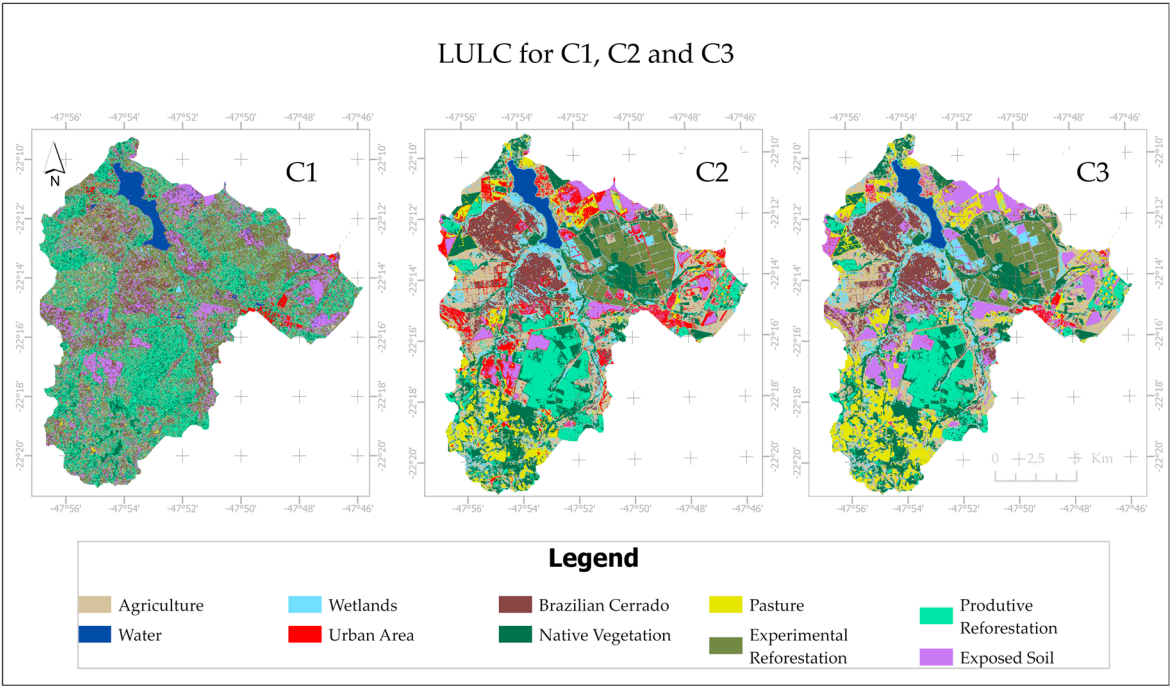


Figure 5. RGB band compositions for C1, C2, and C3.

3.2. LULC and accuracy assessment

The overall accuracy (OA) values attained through RF classification for C1, C2, and C3 were 55.73%, 94.78%, and 96.54%, respectively. Figure 6 depicts the spatial composition of transitional regions between the Brazilian Cerrado and Atlantic Forest interface. The classes identified were agriculture, water, flooded and urban areas, Brazilian Cerrado, native vegetation (Atlantic Forest),

pasture, experimental and productive reforestation, and exposed soil. Figure 7 provides photographic records for each LULC class observed.



**Figure 6.** LULC for C1, C2 and C3 with native vegetation in transition between Brazilian Cerrado and Atlantic Forest interface.

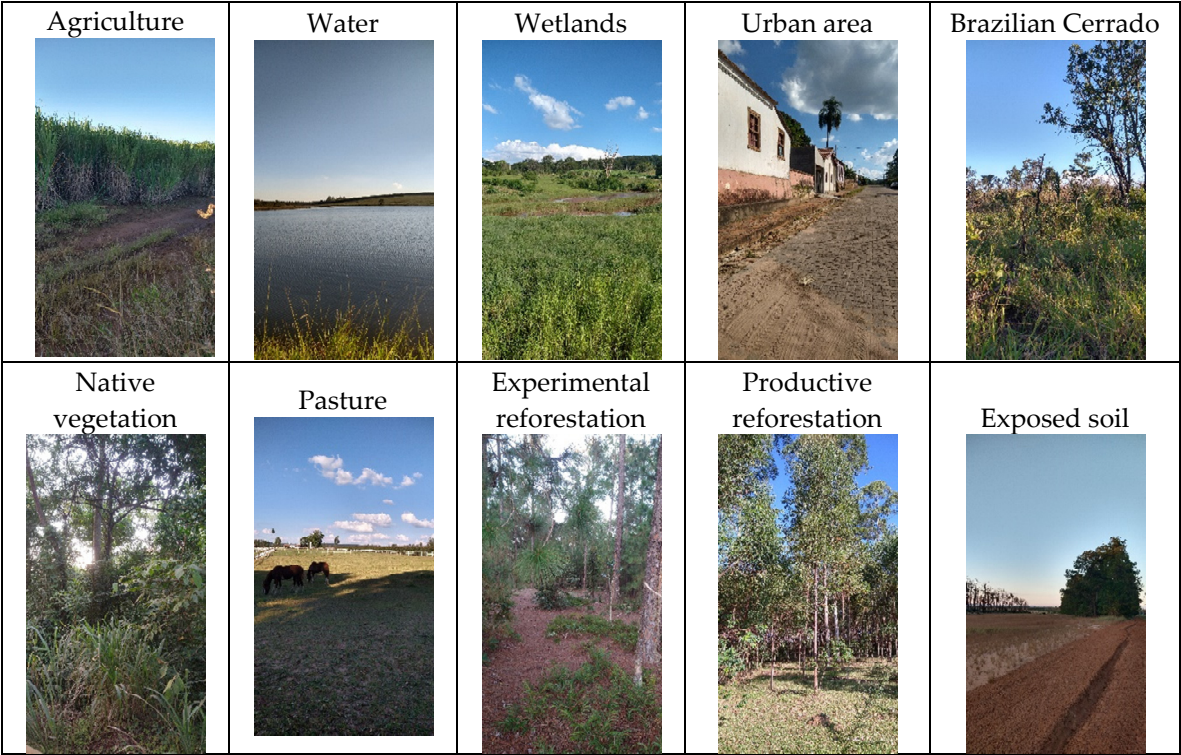


**Figure 7.** Photographic record for each LRHB class.

The accuracy assessment for C1, C2, and C3 used the confusion matrix. Figure 8 presents the producer (PA) and user (UA) accuracy values, omission (OE), and inclusion (IE) errors for each class, as well as the overall accuracy (OA). The results indicate that using only SAR data makes it difficult to attain high PA and UA values for some classes. The agriculture, wetlands, pasture, and Brazilian

Cerrado classes obtained low PA and UA values and, consequently; high OE and IE values, while water and urban area classes attained high accuracy values.

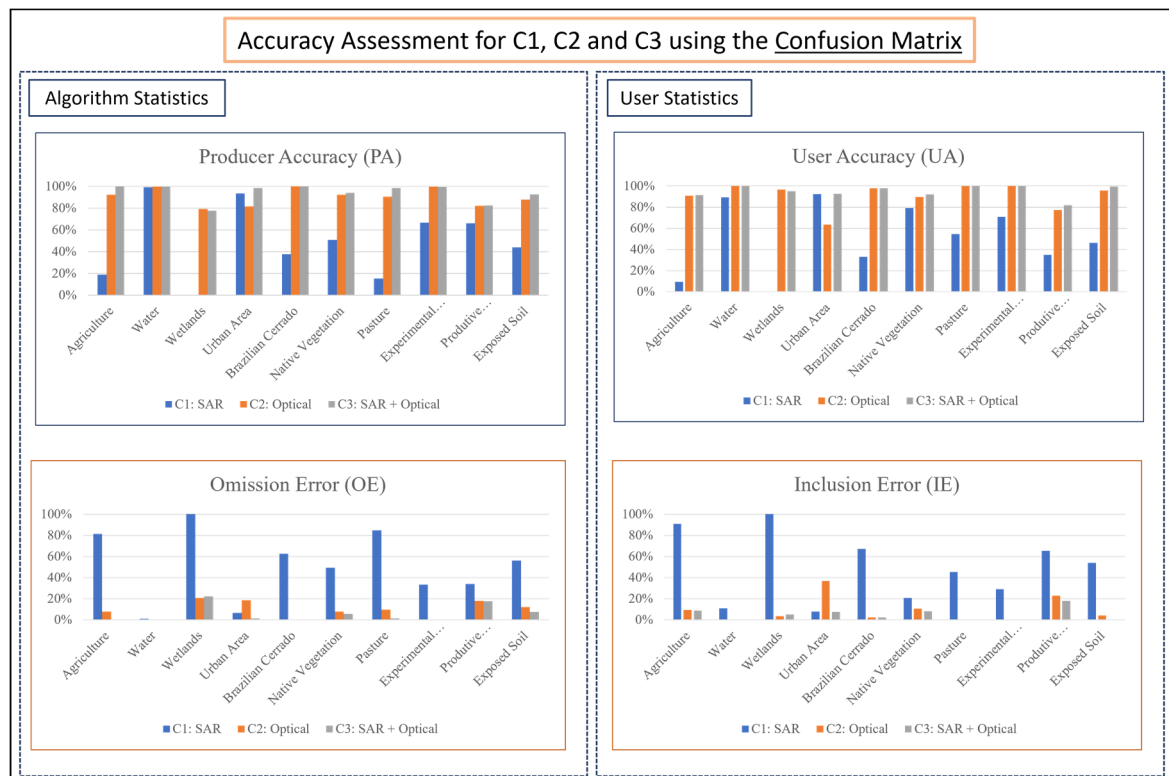


**Figure 8.** Producer and user accuracy values, omission, and inclusion errors for each class for C1, C2, and C3.

As Figure 8 indicates, both C2 and C3 present higher values of OA, PA, and UA than C1. C3, however, modestly exceeded C2, with nearly 2% greater GA, fewer classes with EO and EI, and more classes with higher values of PA and UA, having little difficulty in distinguishing EO in wetlands, productive reforestation, exposed soil, and native vegetation, using the RF algorithm.

#### 4. Discussion

Evaluation of the methodological approach used in this study verifies the integrated use of data from the Sentinel-1 and Sentinel-2 satellites to classify the spatial composition of native vegetation in transitional areas between the Brazilian Cerrado and Atlantic Forest interface. The composition of the basin's native vegetation (Figure 6) is formed by PPAs from the courses of rivers and streams, such as fragments of the Atlantic Forest, PPAs from springs and the region comprising the Itrapina Ecological Station that composed of vegetation characteristic of the savannah and Brazilian Cerrado biome. Mapping such areas comprising the basin's native vegetation types is essential for evaluative studies of water ecosystem services [16], as they play a vital role filtering sediment that would otherwise be deposited in waterways and reservoirs [9,41–43]. In addition, they represent conservation areas that seek to preserve the basin's natural resources [4,26].

The study's analysis of the importance of attributes for LULC classification depicted in Figure 4 indicated that in C1 the most important, in order of descending importance, were the backscatter coefficients ( $\sigma_{VH}^0$  e  $\sigma_{VV}^0$ ), the H- $\alpha$  polarimetric decomposition, and finally the interferometric coherence ( $\gamma_{VH}$  e  $\gamma_{VV}$ ). In C2, the order was B11, B12, B05, B8A, B06, B07, and B08. In C3, the order was that of C2 followed by that of C1.

The C1 confusion matrix demonstrated the difficulties of LULC classification using solely radar data, as it attained the worst values of the three methods examined in the study, achieving only 55.73% OA. The RF algorithm was extremely difficult to classify, confusing the wetlands and water



classes, representing 100% OE and IE. As Figure 3 indicates, the only SAR variable able to differentiate them was the backscatter coefficient  $\sigma^{0}_{VH}$ . The basin's water class is primarily composed of the Lobo Reservoir, drained from the rivers and streams that constitute the basin. However, the waterways limited width make them difficult to distinguish from wetlands of native vegetation in RGB band composition using only radar data (Figure 5). [44], noted that wetlands, in addition to being spatially complex, are temporally variable, and suggest that temporal information from Sentinel-1 has greater discriminatory effectiveness over forested and non-forested wetlands and non-wetlands. While this study did not use time series, it was able to attain sufficient precision for the wetlands class in C3 with 77.78% PA and 94.92% UA, in which all optical data differentiated the two classes quite well and optimized the SAR classification.

In addition, the capacity of  $\sigma^{0}_{VH}$  to distinguish wooded and non-wooded wetlands is related to sensitivity to volume dispersion which largely depends on the vegetative structures of the tree canopy [45]. While this variability is evident in the boxplot graphs, depicting the variables by class (Figure 3), it was not possible to observe the same distinction during the collection of training samples, likely due to the small transitional gradient among the basin's natural characteristics.

Among the difficulties in LULC classification using only SAR data, the RF algorithm did not distinguish pasture well, confusing it with agriculture and Brazilian Cerrado, and attaining 84.73% EO and 45.36% EI. Agriculture was confused with experimental reforestation and exposed soil, attaining 81.18% EO and 90.75% EI. [46], used C-band backscatter coefficient values (RISAT-1) to map rice, vegetation, buildings, and water bodies, through HH and VH polarizations, obtaining 88.57% OA. While [31], mapped the agricultural land, dense vegetation, sparse vegetation, building, fallow, water bodies, and sand classes and obtained 80.27% (OA) accuracy with only backscattering and 87.7% when adding textural variables.

The basin's LULC classes are divided into ten categories (Figure 7) to optimize the mapping of structure of native vegetation (Atlantic Forest and Brazilian Cerrado) and conservation areas (experimental reforestation and wetlands). However, C1 attained only 55.73% OA, with backscatter coefficients its most significant variable (Figure 4). By integrating SAR and optical data, C3 increased OA to 96.54%. The results indicate that while SAR data are widely used because they can differentiate some LULC classes, when used in isolation, they encounter difficulties, for example, in visual interpretation during training. The more classes there are and the greater their distinction, the lower overall accuracy is likely to be, although further research is needed to understand how this works.

The study maps the basin's native vegetation, but C1 encountered difficulties, with the Brazilian Cerrado class registering OE and IE rates of 62.42% and 67.03%, respectively, and was confused with experimental reforestation. In addition, native vegetation class which obtained 49.25% OE and 20.80% IE was confused with productive reforestation. This type of class confusion is reported by other studies as well, [17], observed that the polarimetric decomposition attributes ( $H-\alpha$ ) were crucial in the stratified identification of different classes in the Brazilian Amazon Forest, however, certain similarities were noted in the distribution of forest and field classes.

In Figure 3, the values of entropy and Alpha ( $H-\alpha$ ) for the Brazilian Cerrado were, on average, slightly higher (0.76-0.88) than those for native vegetation (Atlantic Forest) (0.70-0.80) and resemble those of the pasture, wetlands, and experimental reforestation classes. According to [47], this may result from the presence of trees or shrubs in pasture areas, which increase surface roughness, generating a SAR signal like that of forest areas and savannah and grassland forests (Brazilian Cerrado).

[32], noted an increase in mean entropy values (0.6-0.7) in some areas of dry tropical deciduous forests in India, while [17], obtained mean entropy values (0.65-0.75) for Amazon Forest classes. Thus, the SAR variable best able to distinguish Brazilian Cerrado and native vegetation (Atlantic Forest), as well as other classes, was the backscatter coefficient  $\sigma^{0}_{VH}$ , corroborating the results presented in Figure 4. Integrating optical data in classification, the RF algorithm attained PA and UA values of 100% and 97.76%, respectively, for the Brazilian Cerrado and 94.21% and 91.97%, respectively, for native vegetation (Atlantic Forest).



The overall accuracy of 96.54% attained by C 3 conforms with results in other studies integrating SAR and optical data [10,16,21–23,37–39]. [10], evaluated the integrated use of Sentinel-1 and Sentinel-2 data for LULC mapping in a Mediterranean region and attained 90.33% OA. [23], assessed the same data integration for mapping woody plants in savannas and attained 93% OA. Accordingly, the study's objective was achieved, with an overall accuracy slightly better than in some studies [10,16,21–23].

## 5. Conclusions

By evaluating the use of SAR and optical data separately and in an integrated manner, the study demonstrated differences between in pre-processing attributes, classification, and accuracy. Using optical data as variables is easier and faster than using SAR data, particularly in pre-processing. The sole use of either SAR or optical data, however, may fail to meet expectations when a study's objective is complex and may require, for example, a more detailed stratification of LULC classes or obtaining data on days with considerable atmospheric interference. The use of integrated SAR and optical data offers an effective alternative to optimize LULC mapping in tropical regions, due to the low influence of the atmosphere on images in the microwave range.

**Author Contributions:** Allita Rezende dos Santos: Conceptualization, Methodology, Formal analysis, Investigation, Writing—original draft, Writing—review & editing, Funding acquisition. Mariana A. G. A. Barbosa: Conceptualization, Methodology, Formal analysis, Investigation, Writing—review & editing, Funding acquisition. Phelipe da Silva Anjinho: Conceptualization, Methodology, Formal analysis, Investigation, Writing—review & editing, Funding acquisition. Denise Parizotto: Conceptualization, Methodology, Formal analysis, Investigation, Writing—review & editing, Funding acquisition. Frederico Fábio Mauad: Resources, Project administration, Supervision.

**Funding:** We would like to thank the University of São Paulo (USP) and Graduate Program in Environmental Engineering Sciences (PPG-SEA) for funded the APC.

**Acknowledgments:** We would like to thank Coordination of Superior Level Staff Improvement (CAPES) and The National Council for Scientific and Technological Development (CNPq), foundation linked to the Ministry of Science and Technology (MCT) of Brazil, to support this research.

**Conflicts of Interest:** The authors declare no conflict of interest.

## References

1. Akbari, M.; Neamatollahi, E.; Neamatollahi, P. Evaluating Land Suitability for Spatial Planning in Arid Regions of Eastern Iran Using Fuzzy Logic and Multi-Criteria Analysis. *Ecol. Indic.* **2019**, *98*, 587–598, doi:10.1016/j.ecolind.2018.11.035.
2. NEVES, G.L.; GUIMARÃES, T.T.; ANJINHO, P.S.; BARBOSA, M.A.G.A.; SANTOS, A.R. DOS; VIRGENS FILHO, J.S.; MAUAD, F.F. Spatial and Seasonal Assessment of Water Quality in the Lobo Stream River Basin, Brazil Using Multivariate Statistical Techniques. *An. Acad. Bras. Cienc.* **2021**, *93*, doi:10.1590/0001-3765202120210072.
3. Anjinho, P. da S.; Barbosa, M.A.G.A.; Costa, C.W.; Mauad, F.F. Environmental Fragility Analysis in Reservoir Drainage Basin Land Use Planning: A Brazilian Basin Case Study. *Land use policy* **2021**, *100*, 104946, doi:10.1016/j.landusepol.2020.104946.
4. Santos, A.R.; Barbosa, M.A.G.A.; Bolleli, T.; Anjinho, P.S.; Roque, R.; Mauad, F.F. Assessment of Water Ecosystem Integrity (WEI) in a Transitional Brazilian Cerrado–Atlantic Forest Interface. *Water* **2023**, *15*, 775, doi:10.3390/w15040775.
5. Souza, C.M.; Shimbo, J.Z.; Rosa, M.R.; Parente, L.L.; Alencar, A.A.; Rudorff, B.F.T.; Hasenack, H.; Matsumoto, M.; Ferreira, L.G.; Souza-Filho, P.W.M.; et al. Reconstructing Three Decades of Land Use and Land Cover Changes in Brazilian Biomes with Landsat Archive and Earth Engine. *Remote Sens.* **2020**, *12*, 2735, doi:10.3390/RS12172735.
6. Ustaoglu, E.; Aydinoglu, A.C. Suitability Evaluation of Urban Construction Land in Pendik District of Istanbul, Turkey. *Land use policy* **2020**, *99*, 104783, doi:10.1016/j.landusepol.2020.104783.
7. DeFries, R.S.; Floey, J.A.; Asner, G.P. Land-Use Choices: Balancing Human Needs and Ecosystem Function. *Front. Ecol. Environ.* **2004**, *2*, 249–257, doi:10.1890/1540-9295.
8. Tundisi, J.G.; Matsumura-Tundisi, T. The Ecology of UHE Carlos Botelho (Lobo-Broa Reservoir) and Its Watershed, São Paulo, Brazil. *Freshw. Rev.* **2013**, *6*, 75–91, doi:10.1608/frj-6.2.727.

9. Tundisi, J.G.; Tundisi, T.M. Integrating Ecohydrology, Water Management, and Watershed Economy: Case Studies from Brazil. *Ecohydrol. Hydrobiol.* **2016**, *16*, 83–91, doi:10.1016/j.ecohyd.2016.03.006.
10. De Luca, G.; M. N. Silva, J.; Di Fazio, S.; Modica, G. Integrated Use of Sentinel-1 and Sentinel-2 Data and Open-Source Machine Learning Algorithms for Land Cover Mapping in a Mediterranean Region. <https://doi.org/10.1080/22797254.2021.2018667> **2022**, *55*, 52–70, doi:10.1080/22797254.2021.2018667.
11. WWF, W.W.F.F.N. Cerrado, the Brazilian Savanna Available online: [https://wwf.panda.org/discover/knowledge\\_hub/where\\_we\\_work/cerrado/](https://wwf.panda.org/discover/knowledge_hub/where_we_work/cerrado/) (accessed on 19 September 2022).
12. MapBiomias, C. Projeto MapBiomias – Mapeamento Anual de Cobertura e Uso Da Terra No Cerrado - Coleção 7; 2022;
13. MapBiomias, M.A. Projeto MapBiomias – Mapeamento Anual de Cobertura e Uso Da Terra Na Mata Atlântica - Coleção 7; 2022;
14. Santos, A.R. dos; Silva, R.C.F. da; Assis, L.C. de; Mauad, F.F. Defining Environmental Conservation Levels Considering Anthropic Activity in the Uberaba River Basin Protected Area. *Ambient. e Agua - An Interdiscip. J. Appl. Sci.* **2019**, *14*, 1, doi:10.4136/ambi-agua.2279.
15. Maxwell, A.E.; Warner, T.A.; Fang, F. Implementation of Machine-Learning Classification in Remote Sensing: An Applied Review. *Int. J. Remote Sens.* **2018**, *39*, 2784–2817, doi:10.1080/01431161.2018.1433343/SUPPL\_FILE/TRES\_A\_1433343\_SM5998.ZIP.
16. Wen, D.; Ma, S.; Zhang, A.; Ke, X. Spatial Pattern Analysis of the Ecosystem Services in the Guangdong-Hong Kong-Macao Greater Bay Area Using Sentinel-1 and Sentinel-2 Imagery Based on Deep Learning Method. *Sustain.* **2021**, *Vol. 13*, Page 7044 **2021**, *13*, 7044, doi:10.3390/SU13137044.
17. Diniz, J.M.F. de S.; Gama, F.F.; Adami, M. Evaluation of Polarimetry and Interferometry of Sentinel-1A SAR Data for Land Use and Land Cover of the Brazilian Amazon Region. *Geocarto Int.* **2020**, *0*, 1–19, doi:10.1080/10106049.2020.1773544.
18. Eibedingil, I.G.; Gill, T.E.; Scott Van Pelt, R.; Tong, D.Q. Combining Optical and Radar Satellite Imagery to Investigate the Surface Properties and Evolution of the Lordsburg Playa, New Mexico, USA. *Remote Sens.* **2021**, *Vol. 13*, Page 3402 **2021**, *13*, 3402, doi:10.3390/RS13173402.
19. Ienco, D.; Interdonato, R.; Gaetano, R.; Ho Tong Minh, D. Combining Sentinel-1 and Sentinel-2 Satellite Image Time Series for Land Cover Mapping via a Multi-Source Deep Learning Architecture. *ISPRS J. Photogramm. Remote Sens.* **2019**, *158*, 11–22, doi:10.1016/J.ISPRSJPRS.2019.09.016.
20. Morin, D.; Planells, M.; Guyon, D.; Villard, L.; Mermoz, S.; Bouvet, A.; Thevenon, H.; Dejoux, J.F.; Le Toan, T.; Dedieu, G. Estimation and Mapping of Forest Structure Parameters from Open Access Satellite Images: Development of a Generic Method with a Study Case on Coniferous Plantation. *Remote Sens.* **2019**, *Vol. 11*, Page 1275 **2019**, *11*, 1275, doi:10.3390/RS11111275.
21. Nikaein, T.; Iannini, L.; Molijn, R.A.; Lopez-Dekker, P. On the Value of Sentinel-1 InSAR Coherence Time-Series for Vegetation Classification. *Remote Sens.* **2021**, *Vol. 13*, Page 3300 **2021**, *13*, 3300, doi:10.3390/RS13163300.
22. Numbisi, F.N.; Van Coillie, F.M.B.; De Wulf, R.; Be, F.V.; Dewulf@ugent, R.; Be, R.D.W. Delineation of Cocoa Agroforests Using Multiseason Sentinel-1 SAR Images: A Low Grey Level Range Reduces Uncertainties in GLCM Texture-Based Mapping. *ISPRS Int. J. Geo-Information* **2019**, *Vol. 8*, Page 179 **2019**, *8*, 179, doi:10.3390/IJGI8040179.
23. Zhang, W.; Brandt, M.; Wang, Q.; Prishchepov, A. V.; Tucker, C.J.; Li, Y.; Lyu, H.; Fensholt, R. From Woody Cover to Woody Canopies: How Sentinel-1 and Sentinel-2 Data Advance the Mapping of Woody Plants in Savannas. *Remote Sens. Environ.* **2019**, *234*, 111465, doi:10.1016/J.RSE.2019.111465.
24. Fang, B.; Li, Y.; Zhang, H.; Chan, J.C.W. Collaborative Learning of Lightweight Convolutional Neural Network and Deep Clustering for Hyperspectral Image Semi-Supervised Classification with Limited Training Samples. *ISPRS J. Photogramm. Remote Sens.* **2020**, *161*, 164–178, doi:10.1016/J.ISPRSJPRS.2020.01.015.
25. Campregher, R.; Martins, R.C. O “Modelo Broa” e a Produção de Conhecimento Científico Sobre o Meio Ambiente. *Desenvolv. e Meio Ambient.* **2017**, *40*, 141–158, doi:10.5380/dma.v40i0.49243.
26. Santos, A.R. dos; Anjinho, P. da S.; Neves, G.L.; Barbosa, M.A.G.A.; de Assis, L.C.; Mauad, F.F. Dynamics of Environmental Conservation: Evaluating the Past for a Sustainable Future. *Int. J. Appl. Earth Obs. Geoinf.* **2021**, *102*, 102452, doi:10.1016/j.jag.2021.102452.
27. São Paulo, G. do E. de Declara Área de Proteção Ambiental Regiões Situadas Em Diversos Municípios, Dentre Os Quais Corumbatai, Botucatu e Tejuca; Brasil, 1983;
28. IF, I.F. do E. de S.P. Plano de Manejo Integrado Das Estações Ecológica e Experimentnal de Itirapina/SP; 2006;
29. ESA, E.S.A. Copernicus Open Access Hub Available online: <https://scihub.copernicus.eu/dhus/#/home> (accessed on 24 April 2023).
30. United States Geological Survey, U. Digital Elevation Model (DEM), Advanced Spaceborne Thermal Emission and Reflect-Tion Radiometer (ASTER). *Copernicus Open Access Hub Eur. Sp. Agency* **2015**.

31. Mishra, V.N.; Prasad, R.; Rai, P.K.; Vishwakarma, A.K.; Arora, A. Performance Evaluation of Textural Features in Improving Land Use/Land Cover Classification Accuracy of Heterogeneous Landscape Using Multi-Sensor Remote Sensing Data. *Earth Sci. Informatics* **2019**, *12*, 71–86, doi:10.1007/S12145-018-0369-Z/TABLES/10.
32. Varghese, A.O.; Suryavanshi, A.; Joshi, A.K. Analysis of Different Polarimetric Target Decomposition Methods in Forest Density Classification Using C Band SAR Data. <http://dx.doi.org/10.1080/01431161.2015.1136448> **2016**, *37*, 694–709, doi:10.1080/01431161.2015.1136448.
33. Cloude, S. The Dual Polarization Entropy/Alpha Decomposition: A PALSAR Case Study. *ESASP* **2007**, *644*, 2.
34. Lee, J. Sen Digital Image Enhancement and Noise Filtering by Use of Local Statistics. *IEEE Trans. Pattern Anal. Mach. Intell.* **1980**, *PAMI-2*, 165–168, doi:10.1109/TPAMI.1980.4766994.
35. Belgiu, M.; Drăgu, L. Random Forest in Remote Sensing: A Review of Applications and Future Directions. *ISPRS J. Photogramm. Remote Sens.* **2016**, *114*, 24–31, doi:10.1016/J.ISPRSJPRS.2016.01.011.
36. Breiman, L. Random Forests. *Mach. Learn.* **2001**, *45*, 5–32, doi:10.1023/A:1010933404324/METRICS.
37. Foody, G.M. Status of Land Cover Classification Accuracy Assessment. *Remote Sens. Environ.* **2002**, *80*, 185–201, doi:10.1016/S0034-4257(01)00295-4.
38. Foody, G.M. Explaining the Unsuitability of the Kappa Coefficient in the Assessment and Comparison of the Accuracy of Thematic Maps Obtained by Image Classification. *Remote Sens. Environ.* **2020**, *239*, 111630, doi:10.1016/J.RSE.2019.111630.
39. Story, M.; Congalton, R.G. Accuracy Assessment: A User's Perspective. *Photogramm. Eng. Remote Sensing* **1986**, *52*, 397–399.
40. Heidarlou, H.B.; Shafiei, A.B.; Erfanian, M.; Tayyebi, A.; Alijanpour, A. Effects of Preservation Policy on Land Use Changes in Iranian Northern Zagros Forests. *Land use policy* **2019**, *81*, 76–90, doi:10.1016/j.landusepol.2018.10.036.
41. Calijuri, M.L.; Castro, J. de S.; Costa, L.S.; Assemany, P.P.; Alves, J.E.M. Impact of Land Use/Land Cover Changes on Water Quality and Hydrological Behavior of an Agricultural Subwatershed. *Environ. Earth Sci.* **2015**, *74*, 5373–5382, doi:10.1007/s12665-015-4550-0.
42. Mishra, P.K.; Rai, A.; Rai, S.C. Land Use and Land Cover Change Detection Using Geospatial Techniques in the Sikkim Himalaya, India. *Egypt. J. Remote Sens. Sp. Sci.* **2020**, *23*, 133–143, doi:10.1016/j.ejrs.2019.02.001.
43. Periotto, N.A.; Tundisi, J.G. Serviços Ecossistêmicos Do Reservatório Da UHE Carlos Botelho (Lobo-Broa): Uma Nova Abordagem Para o Gerenciamento e Planejamento Dos Múltiplos Usos de Represas. *Brazilian J. Biol.* **2013**, *73*, 471–482, doi:10.1590/S1519-69842013000300003.
44. Li, Z.; Chen, H.; White, J.C.; Wulder, M.A.; Hermosilla, T. Discriminating Treed and Non-Treed Wetlands in Boreal Ecosystems Using Time Series Sentinel-1 Data. *Int. J. Appl. Earth Obs. Geoinf.* **2020**, *85*, 102007, doi:10.1016/J.JAG.2019.102007.
45. Freeman, A.; Durden, S.L. A Three-Component Scattering Model for Polarimetric SAR Data. *IEEE Trans. Geosci. Remote Sens.* **1998**, *36*, 963–973, doi:10.1109/36.673687.
46. Mishra, V.N.; Prasad, R.; Kumar, P.; Srivastava, P.K.; Rai, P.K. Knowledge-Based Decision Tree Approach for Mapping Spatial Distribution of Rice Crop Using C-Band Synthetic Aperture Radar-Derived Information. *J. Appl. Remote Sens.* **2017**, *11*, 1, doi:10.1117/1.JRS.11.046003.
47. Delgado-Aguilar, M.J.; Fassnacht, F.E.; Peralvo, M.; Gross, C.P.; Schmitt, C.B. Potential of TerraSAR-X and Sentinel 1 Imagery to Map Deforested Areas and Derive Degradation Status in Complex Rain Forests of Ecuador. *Int. For. Rev.* **2017**, *19*, 102–118, doi:10.1505/146554817820888636.

**Disclaimer/Publisher's Note:** The statements, opinions and data contained in all publications are solely those of the individual author(s) and contributor(s) and not of MDPI and/or the editor(s). MDPI and/or the editor(s) disclaim responsibility for any injury to people or property resulting from any ideas, methods, instructions or products referred to in the content.